



# Quantifying hard coal mines CH<sub>4</sub> emissions from TROPOMI and IASI observations using high-resolution CAMS forecast data and the wind-assigned anomaly method

Qiansi Tu<sup>1</sup>, Matthias Schneider<sup>1</sup>, Frank Hase<sup>1</sup>, Farahnaz Khosrawi<sup>1</sup>, Benjamin Ertl<sup>1,2</sup>, Jaroslaw Necki<sup>3</sup>,  
5 Darko Dubravica<sup>1</sup>, Christopher J. Diekmann<sup>1</sup>, Thomas Blumenstock<sup>1</sup>, Dianjun Fang<sup>4</sup>

<sup>1</sup> Karlsruhe Institute of Technology (KIT), Institute of Meteorology and Climate Research (IMK-ASF), Karlsruhe, Germany

<sup>2</sup> Karlsruhe Institute of Technology, Steinbuch Centre for Computing (SCC), Karlsruhe, Germany

<sup>3</sup> AGH – University of Science and Technology, Krakow, Poland

<sup>4</sup> School of Mechanical Engineering, Tongji University, Shanghai, China

10

*Correspondence to:* Qiansi Tu (qiansi.tu@kit.edu), Matthias Schneider (matthias.schneider@kit.edu)

**Abstract.** Intensive coal mining activities are in the Upper Silesian Coal Basin (USCB) in southern Poland, resulting in large amounts of methane (CH<sub>4</sub>) emissions. Annual CH<sub>4</sub> emission reached to 448 kt according to the European Pollutant Release and Transfer Register (E-PRTR, 2017). As a CH<sub>4</sub> emission hot spot in Europe, it is of importance to investigate its emission  
15 sources and accurate emission estimates.

In this study, we use satellite-based column-averaged dry-air molar fraction observations of CH<sub>4</sub> (XCH<sub>4</sub>) from the TROPospheric Monitoring Instrument (TROPOMI) and tropospheric XCH<sub>4</sub> (TXCH<sub>4</sub>) from the Infrared Atmospheric Sounding Interferometer (IASI), together with the high-resolution model forecast XCH<sub>4</sub> and TXCH<sub>4</sub> from the Copernicus Atmosphere Monitoring Service (CAMS) to estimate the CH<sub>4</sub> emission rate averaged over three years in the USCB region  
20 (49.3° - 50.8° N and 18° - 20° E). Using the CAMS inventory as the a priori knowledge of the sources, together with ERA5 wind at 330 m, the wind-assigned XCH<sub>4</sub> anomalies for two opposite wind directions are calculated, which yields an estimated CH<sub>4</sub> emission of  $9.6E26 \pm 1.4E25$  molec./s for CAMS XCH<sub>4</sub> and  $9.1E26 \pm 1.2E25$  molec./s for CAMS TXCH<sub>4</sub>. These values are very close to the total emission of the CAMS inventory ( $9.7E26$  molec./s). Very good agreements between CAMS and the  
25 similar estimates of XCH<sub>4</sub> and TXCH<sub>4</sub> also imply that for a strong source, the dynamically induced variations of the CH<sub>4</sub> mixing ratio in the upper troposphere and lower stratosphere region is of secondary importance.

This wind-assigned method is further applied to the TROPOMI XCH<sub>4</sub> and TROPOMI+IASI TXCH<sub>4</sub> with using the Carbon dioxide and Methane (CoMet) inventory performed in 2018. The calculated averaged total CH<sub>4</sub> emission over the USCB region is about  $5.7E26 \pm 4.9E24$  molec./s for TROPOMI XCH<sub>4</sub> and  $5.2E26 \pm 2.2E25$  molec./s for TROPOMI+IASI TXCH<sub>4</sub>. These  
30 results are very close and thus in agreement to the emissions given in the E-PRTR inventory ( $5.33E26$  molec./s) and the CoMet inventory ( $6.6E26$  molec./s).



Since the wind speed is increasing with altitude, sensitivity tests show that higher CH<sub>4</sub> emission strengths are yielded with increasing altitude and vice versa. About 23% lower and 13% higher estimates are obtained when using lower wind information at 10 m and higher wind information at 500 m instead of 330 m, respectively. When using different wind coverage and different wind segmentation, an uncertainty of 4.2% and -2.1% is obtained, respectively. These results suggest that our wind-assigned method is quite robust and might also serve as a simple method to estimate CH<sub>4</sub> or CO<sub>2</sub> emissions for other regions.

## 1 Introduction

Atmospheric methane (CH<sub>4</sub>) is the second most important anthropogenic greenhouse gas (GHG) with a larger global warming potential than carbon dioxide (CO<sub>2</sub>) (IPCC, 2014). The globally averaged amount of atmospheric CH<sub>4</sub> has increased by 260% to 1877 ± 2 ppb from the preindustrial era to 2019 (World Meteorological Organization, 2020). Methane sources induced by anthropogenic activities include fossil fuel production and use (e.g., coal mining, gas/oil extraction), and waste disposal and agriculture, which in total accounts for about 60% of the total CH<sub>4</sub> emissions (Saunois et al., 2020). Although most sources and sinks of CH<sub>4</sub> have been characterized, their spatial-temporal variations and relative contributions to the atmosphere CH<sub>4</sub> level are still highly uncertain (Kirschke et al., 2013; Saunois et al., 2020).

Approximately 33% of the CH<sub>4</sub> emissions from coal mining (43 TgCH<sub>4</sub>yr<sup>-1</sup>) are estimated to come from the total fossil-fuel-related emissions during 2008-2017 (Saunois et al., 2020). CH<sub>4</sub> is released primarily to the atmosphere via ventilation shafts located at the surface during the production and processing of the coal (Saunois et al., 2020; Andersen et al. 2021). The largest contribution of CH<sub>4</sub> emission related with the coal mining activities in Europe is from southern Poland—the Upper Silesian Coal Basin (USCB) (Luther et al, 2019; Krautwurst et al., 2021). The European Pollutant Release and Transfer Register (E-PRTR, 2017; <https://prtr.eea.europa.eu/>, last access: 25 October 2021) reports that the total CH<sub>4</sub> emissions from the USCB region amount to 448 kt yr<sup>-1</sup> (5.33E26 molec./s). Most of these emissions are from mining activities and heavy industry (Kostinek et al., 2021), which makes this region a hot spot of CH<sub>4</sub> emission in Europe. To investigate the CH<sub>4</sub> emission from this hot spot, the Carbon Dioxide and Methane (CoMet) campaign was performed, covering roughly 3 weeks from May to June 2018 (more details can be found in Luther et al, 2019; Fiehn et al., 2020; Kostinek et al., 2021; Krautwurst et al., 2021). Many studies present similar CH<sub>4</sub> emission estimates for the region based on different instruments and methods. Luther et al. (2019) estimated CH<sub>4</sub> emissions ranging from 6 ± 1 kt yr<sup>-1</sup> (7.14E24 ± 1.19E24 molec./s) for a single shaft to up to 109 ± 33 kt yr<sup>-1</sup> (1.30E26 ± 3.92E25 molec./s) for a subregion of the USCB, by using several portable Fourier Transform Infrared (FTIR) spectrometers (Bruker EM27/SUN). Fiehn et al (2020) analyzed aircraft- and ground-based in situ observations and reported an emission estimate of 436 ± 115 kt yr<sup>-1</sup> (5.19E26 ± 1.37E26 molec./s) and 477 ± 101 kt yr<sup>-1</sup> (5.68E26 ± 1.20E26 molec./s) from two selected flights. An advanced model approach was introduced by Kostinek et al. (2021) to investigate two research flights in the morning and afternoon, resulting in estimated CH<sub>4</sub> emissions of 451 ± 77 kt yr<sup>-1</sup> (5.37E26 ± 9.16E25 molec./s) and 423 ± 79 kt yr<sup>-1</sup> (5.03E26 ± 9.40E25 molec./s), respectively. Another emission estimate based on the observations from the nadir-looking passive remote sensing Methane Airborne MAPper (MAMAP) instrument accounted for



8.8 kt yr<sup>-1</sup> (1.05E25 molec./s) to 78.8 kt yr<sup>-1</sup> (9.38E25 molec./s) for a sub-clusters of ventilation shafts (Krautwurst et al.,  
65 2021). A recent study (Luther et al., 2021) displays a larger emission rate of 414 – 790 kt yr<sup>-1</sup> (4.9E26 – 9.4E26 molec./s)  
based on a network of four portable FTS instrument (EM27/SUN) during the CoMet campaign.

Launched in October 2017, the TROPOspheric Monitoring Instrument (TROPOMI) on board the Sentinel-5 Precursor  
satellite provides an unprecedented high spatial resolution (5.5 × 7 km<sup>2</sup>) of the CH<sub>4</sub> total column-averaged dry-air mole fraction  
(XCH<sub>4</sub>) (Veefkind et al., 2012; Lorente et al., 2021). An a posteriori method has been developed by Schneider et al. (2021) to  
70 obtain tropospheric XCH<sub>4</sub> by combining observations from TROPOMI and the Infrared Atmospheric Sounding Interferometer  
(IASI). This synergetic combination product is not influenced by the changing tropopause height, and it offers improved  
sensitivity to the tropospheric variations than the total column XCH<sub>4</sub> data from either sensor. The improved real-time forecast  
data with high resolution (0.1° × 0.1°~9 km × 9km) are produced by the Copernicus Atmosphere Monitoring Service (CAMS)  
(Agustí-Panareda et al., 2019; Barré et al., 2021). All the data sets provide a large coverage and long-term XCH<sub>4</sub>/TXCH<sub>4</sub>  
75 observations, which helps to better estimate CH<sub>4</sub> emission in the USCB region.

In Sect. 2 we present the data sets and methodology used in this study to derive estimated CH<sub>4</sub> emissions. The results and  
discussions are presented in Sect. 3. We present a novel wind-assigned method introduced by Tu et al., 2021, which is firstly  
verified by the CAMS model forecasts and then applied to the TROPOMI XCH<sub>4</sub> and TROPOMI+IASI TXCH<sub>4</sub> data to estimate  
the CH<sub>4</sub> emissions in the USCB region, together with an uncertainty analysis. Finally, the summary and conclusions are given  
80 in Sect. 4.

## 2 Data sets and method

There are over 50 active ventilation shafts in the USCB region (49.3° - 50.8° N and 18° - 20° E), Poland, whose emission rates  
range between 2E23 molec./s and 5E25 molec./s (Gałkowski et al, 2021) (Figure 4b). Most of them are located near Katowice  
and further west and southwest of Katowice.

### 85 2.1 CAMS CH<sub>4</sub> forecast and emission inventories

The Integrated Forecasting System (IFS, <https://www.ecmwf.int/en/publications/ifs-documentation>, last access: 27 October,  
2021) from the European Centre for Medium-Range Weather Forecasts (ECMWF) is used in the CAMS atmospheric  
composition analysis and forecasts system to simulate five-day CO<sub>2</sub> and CH<sub>4</sub> forecasts (Agustí-Panareda et al., 2019, Barré et  
al., 2021), as well as other chemical species and aerosol (Flemming et al., 2015; Morcrette et al., 2009). This model is also  
90 used in the operational Numerical Weather Prediction (NWP) system, but with additional modules (Agustí-Panareda et al.,  
2019). The forecast data used in this study is the same suit as the one used in Barré et al. (2021), where the Cycle 45r1 IFS  
model cycle was implemented. The CAMS GHGs operational dataset include analysis and forecasts at medium and high  
resolution with 137 model levels from the surface to 0.01 hPa (Barré et al., 2021). In this study we will focus on using the  
high-resolution CH<sub>4</sub> forecasts, which have a spatial resolution of 0.1° × 0.1° and a temporal resolution of 3h, starting from



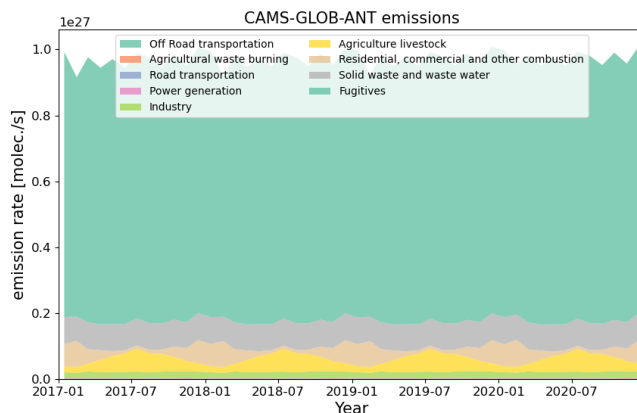
95 00:00 UTC. Here we use the daily averaged CAMS forecasts during 9:00 UTC - 18:00 UTC at each resolution grid point. The corresponding standard deviation (STD) is considered as the noise/error:

$$STD = \frac{\sum_{i=1}^n (XCH_{4i} - \overline{XCH_4})^2}{\sqrt{n}} \quad \text{Eq. 1}$$

where  $XCH_{4i}$  is the CAMS  $XCH_4$  (or CAMS  $TXCH_4$ ) in each resolution grid at each time step,  $\overline{XCH_4}$  is the daily average (9:00 UTC - 18:00 UTC), and  $n$  is the number of CAMS forecasts of each day. The time resolution of CAMS forecasts is 3h and thus,  $n = 4$ .

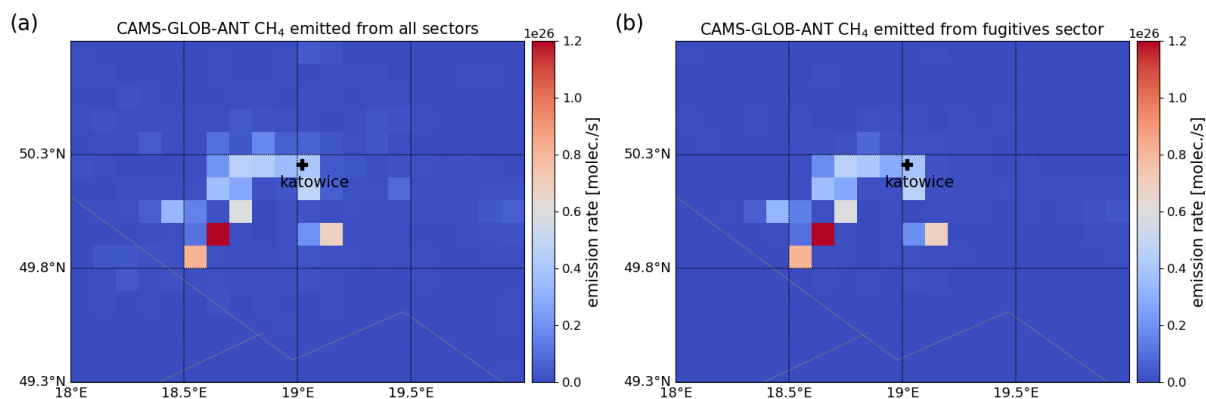
100 The anthropogenic methane emissions used in the global CAMS forecasts are from the CAMS global anthropogenic emission inventory (CAMS-GLOB-ANT, <https://permalink.aeris-data.fr/CAMS-GLOB-ANT>, last access: 27 October, 2021). The CAMS-GLOB-ANT inventory is based on the emissions provided by the EDGARv4.3.2 inventory for the time period 2000-2012 (Crippa et al., 2018) and linearly extrapolated to 2020 using the trends from the CEDA global inventory in 2011-2014 (Hoesly et al., 2018). The latest version (CAMS-GLOB-ANT v4.2) was released in March 2020, using the same set-up  
105 as v4.1 except for adding the emissions in 2020. The anthropogenic sources in the standard v4.2 are divided into 12 sectors and the agriculture sections are split into three sectors, including livestock, soils and waste burning (<https://eccad3.sedoo.fr/>, last access: 27 October, 2021). The inventory is provided as monthly mean with the same spatial resolution ( $0.1^\circ \times 0.1^\circ$ ) as the CAMS forecast data (Granier et al., 2019).

The monthly averages of the CAMS global anthropogenic emissions for different sectors in the study area of USCB are  
110 presented in Figure 1. The emissions from the sectors “agriculture soils” and “solvents” are zeros, and emissions from ships with a magnitude of 19 are much lower than the other sectors. Thus, these three sectors are not shown here. The fugitive sources tend to be from energy production and distribution (e.g. fuel use) and are the dominant  $CH_4$  sources in this region with a mean value of  $7.9E26$  molec./s and a standard deviation of  $2.2E25$  molec./s. Compared to its high amount, the seasonal variations of the fugitives sector can be ignored. Though the sources from agriculture livestock ( $1.7E25 \pm 4.0E25$  molec./s)  
115 show an obvious seasonal cycle, these amount only 4% of the total emissions in this region. Whereas the  $CH_4$  emitted from the fugitives sector occupies 82%. The spatial distribution of the  $CH_4$  inventory of the CAMS-GLOB-ANT from all anthropogenic sources and from fugitives are quite similar in the USCB region (Figure 2). Therefore, we apply the three-year mean of total emissions at grids with significant emissions without considering seasonal variations in the simple plume model (see Sect. 2.3). The total emissions amount to  $9.7E26$  molec./s over this study area.



120

**Figure 1: Different sectors of the monthly averaged CAMS global anthropogenic emissions ( $>1E20$  molec./s) in the USCB region for 2017-2020 (<https://permalink.aeris-data.fr/CAMS-GLOB-ANT>, last access: 22 December 2021. Granier et al., 2019)**



125

**Figure 2: Spatial distribution of the CAMS global anthropogenic emissions over the USCB region on a  $0.1^\circ \times 0.1^\circ$  latitude/longitude grid from (a) all sectors and (b) the fugitives sector. The fugitives are the dominant  $CH_4$  sources.**

## 2.2 TROPOMI and IASI data sets

The TROPOMI instrument is a nadir-viewing, imaging spectrometer, which uses passive remote sensing techniques to perform measurements of the solar radiation reflected by and radiated from the earth in the ultraviolet, the visible, the near-infrared and the shortwave infrared spectral bands (Veeffkind et al., 2012). The algorithm for  $CH_4$  column retrieval is called RemoTeC algorithm and it has been extensively used to derive  $CO_2$  and  $CH_4$  retrievals from Greenhouse Gases Observing Satellite (GOSAT) and Orbiting Carbon Observatory-2 (OCO-2; Boesch et al., 2011; Butz et al., 2009, 2011; Hasekamp and Butz, 2008; Schepers et al., 2012). An updated retrieval algorithm has been implemented by Lorente et al. (2021) to obtain a data suit with less scatter and a higher resolution surface altitude database. This updated TROPOMI  $XCH_4$  dataset has been validated with the Total Carbon Column Observing Network (TCCON) ( $-3.4 \pm 5.6$  ppb) and GOSAT ( $-10.3 \pm 16.8$  ppb),

130



135 showing very good agreements. In this study the TROPOMI XCH<sub>4</sub> during November 2017 and December 2020 within the  
study area over the USCB region is investigated. The data provided by Lorente et al. (2021) includes an additional quality  
filter parameter (quality value, q). TROPOMI XCH<sub>4</sub> with qa=1.0 represents the data under clear-sky and low-cloud  
atmospheric conditions and the problematic data points are removed as well, which is applied in this study.

The IASI instrument is a nadir viewing Fourier-transform spectrometer that measures the infrared part of the electromagnetic  
140 spectrum. IASI measurements are performed with a horizontal resolution of 12 km and a full swath width of about 2200 km  
on the ground. It is the key payload element of the polar-orbiting Metop-A -B and -C satellites. These satellites overpass the  
equator at 09:30 in the morning and 21:30 local time in the evening with a little more than 14 orbits per day. It provides  
unprecedented accurate vertical information of the atmospheric temperature and humidity, which helps to improve numerical  
weather prediction (NWP). The thermal infrared nadir spectra of IASI have been successfully used in retrieving different  
145 atmospheric trace gas profiles and these retrievals are especially sensitive between the middle troposphere and the stratosphere  
(Schneider et al., 2021). By combining these IASI profiles and the TROPOMI CH<sub>4</sub> total column which has a higher sensitivity  
near ground, it is able to detect the tropospheric XCH<sub>4</sub> (TXCH<sub>4</sub>) independently from CH<sub>4</sub> at higher altitudes. The combined  
product cannot be obtained by either the TROPOMI or IASI product independently. It shows a weak positive bias of about 1  
% with respect to the references (Schneider et al., 2021). We refer to this product in the following as the TROPOMI+IASI  
150 TXCH<sub>4</sub>.

### 2.3 Simple plume model and wind-assigned anomaly method

The averaged distribution of emitted CH<sub>4</sub> over a long-term period can be modeled simply as an evenly-distributed cone-shape  
dispersion based on the wind and source strength. Since CH<sub>4</sub> is a long-lived gas, its decay is negligible for short periods and  
not considered in the model. This model is referred to as simple plume model (see Figure 2, Tu et al., 2021). We use the model  
155 wind from ERA5, which is the fifth generation ECMWF reanalysis product using 4D-Var data assimilation and model forecasts  
in Cycle 41R2 of the ECMWF IFS model (Copernicus Climate Change Service, C3S, 2017, Hersbach et al., 2020). It provides  
hourly estimates on 137 pressure levels in the vertical covering the atmosphere from the surface up to 0.01 hPa, with a spatial  
resolution of 0.25°×0.25° (Hersbach et al., 2020).

Based on the simple plume model, the enhanced CH<sub>4</sub> column ( $\Delta\text{CH}_4$ ) at the downwind side of the location ( $x_i, y_i$ ) is  
160 computed as:

$$\Delta\text{CH}_4(x_i, y_i) = \frac{\varepsilon}{v \cdot d(x_i, y_i) \cdot \alpha} \quad \text{Eq. 2}$$

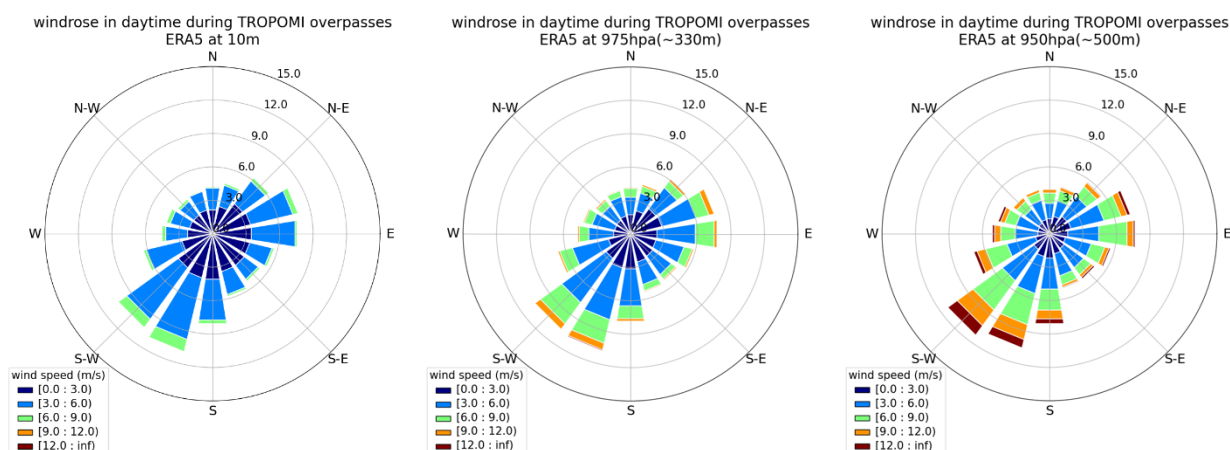
where the emission strength  $\varepsilon$  is the a priori knowledge from the CAMS-GLOB-ANT data set or from the coal mine ventilation  
shafts in this study (see Sect. 3.2). Their emission rates are assumed to be constant with time from 2017 to 2020.  $\alpha$  is the angle  
of the emission cone and has an empirical value of 60°.  $v$  is the wind speed from ERA5, and  $d$  is the distance between the  
downwind location and the CH<sub>4</sub> emission source. Each individual source either from the CAMS-GLOB-ANT inventory or



165 from the knowledge of the ventilation shafts is considered as an individual point source. The plumes computed from different point sources over daytime (8:00 UTC - 18:00 UTC) are super-positioned and then averaged to a daily plume.

The wind distributions at different height levels (10 m, ~330 m, ~500 m) over the USCB region are presented in Figure 3. The wind speed increases with increasing altitude (see Table A-1). The ERA5 wind is divided into two opposite wind regimes based on directions (e.g., 135°-315° for SW and the rest for NE). For each wind sector, an averaged plume is computed and the difference of the two plumes are therefore the wind-assigned anomalies. The estimated emission strengths can be calculated by fitting the modelled anomalies to the known anomalies from e.g. CAMS XCH<sub>4</sub>/TXCH<sub>4</sub>, and TROPOMI and TROPOMI+IASI observations. Note that CH<sub>4</sub> has a lifetime of around 12 years, which results in a high background compared to the newly emitted CH<sub>4</sub>. Thus, the contributions from the background should be removed for correctly estimating emissions (Liu et al., 2021). The background is considered to consist of a constant value, a linear increase with time, a seasonal cycle, a daily anomaly and a horizontal anomaly. For more details, see the Appendix in Tu et al., 2021.

175 This method was firstly used to estimate the CH<sub>4</sub> emission from landfills in Madrid, Spain and yielded a CH<sub>4</sub> emission rate of  $7.4 \times 10^{25} \pm 6.4 \times 10^{24}$  molec./s based on the TROPOMI XCH<sub>4</sub> (Tu et al., 2021).



180 **Figure 3: Windrose plots for daytime (08:00 UTC – 18:00 UTC) from November 2017 to December 2020 for the ERA5 model wind at different vertical levels (10 m, ~330 m and ~500m). The days for the three year average coincide with the TROPOMI overpass days.**

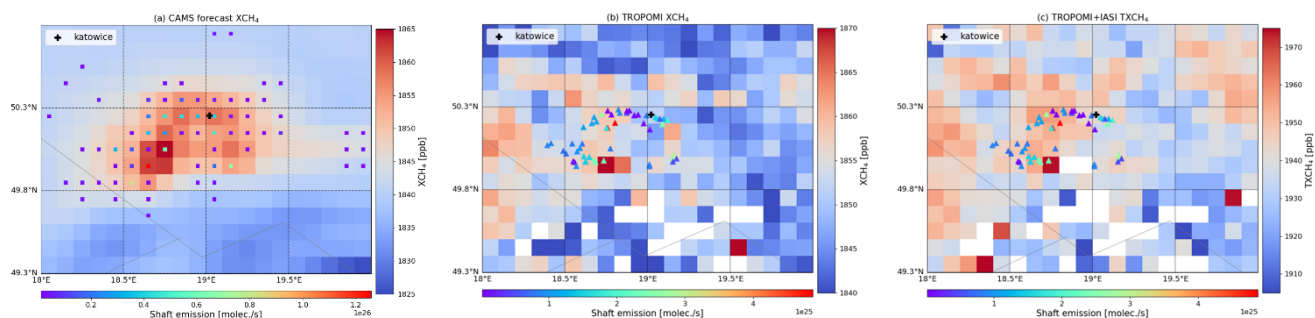
### 3. Results and discussion

#### 3.1 Estimated emissions derived from CAMS forecasts (evaluation of the method)

The CAMS forecast XCH<sub>4</sub> data from November 2017 to December 2020 within the study area are illustrated in Figure 4 left. The areas with high XCH<sub>4</sub> amounts fit well with the CAMS anthropogenic CH<sub>4</sub> emissions (square symbols). Similar to the CoMet inventory, high sources in the CAMS-GLOB-ANT inventory are centered in this region, but there are other weaker sources outside. The total emission rate of the CoMet inventory is  $6.6E26$  molec./s, which is slightly less than the CAMS-



GLOB-ANT emissions ( $9.7E26$  molec./s). This is probably because the CAMS inventory includes more  $CH_4$  emission sources, e.g., wastes, and combustion from residential, commercial, which account to about 20%.



190

**Figure 4: (a) CAMS forecast, (b) TROPOMI  $XCH_4$  and (c) TROPOMI+IASI  $TXCH_4$  in the USCBA region on a  $0.1^\circ \times 0.1^\circ$  latitude/longitude grid during November 2017–December 2020. The square and triangle symbols represent the locations of CAMS-GLOB-ANT sources (for a better viewing, only the emission strengths larger than  $1E24$  molec./s are shown here) and the active coal mine shafts from the CoMet inventory (Galkowski et al, 2021), respectively. Different colors denote the amount of emission rates.**

195 Based on the CAMS emissions, the wind-assigned method is applied to CAMS  $XCH_4$ . The  $XCH_4$  anomalies (raw-background) and the wind-assigned anomalies are presented in Figure 5a and b, respectively. Note, that the CAMS  $XCH_4$  is coincided with TROPOMI  $XCH_4$  for better comparison. Some data are thus missing here mostly due to the quality filter of TROPOMI observations. After removing the  $XCH_4$  background, the  $XCH_4$  anomalies well represent the CAMS sources. The highest  $CH_4$  sources from the CAMS-GLOB-ANT inventory are also obviously seen in the 2D anomalies. In addition, the spatial distributions of the three  $XCH_4$  data products show different patterns (Figure 4), whereas the anomalies (after removing background) patterns are similar (Figure 5(a) and (d), Figure 7(a) and (d)). This indicates that the background removal is of importance for  $XCH_4$  and our method works well.

200

The CAMS  $\Delta XCH_4$  and modelled  $\Delta XCH_4$  show a very good agreement with a slope of 0.97 and a  $R^2$  of 0.89 (Figure 5c). Our results are derived from the CAMS emission information, and they agree very good with the CAMS model data. The estimated emission rate is about  $9.6E26 \pm 1.4E25$  molec./s when using the ERA5 wind at 975 hPa ( $\sim 330$  m) and this value is very close to the CAMS inventory (estimated emission rate at other levels are presented in Sec. 3.2). Therefore, we use ERA5 wind at this level in the following. Note that the points whose distances to the nearest dominant sources are less than 10 km, are removed here, because they are very close to the significant sources and small changes in wind (either speed or direction) can result in high uncertainties.

205

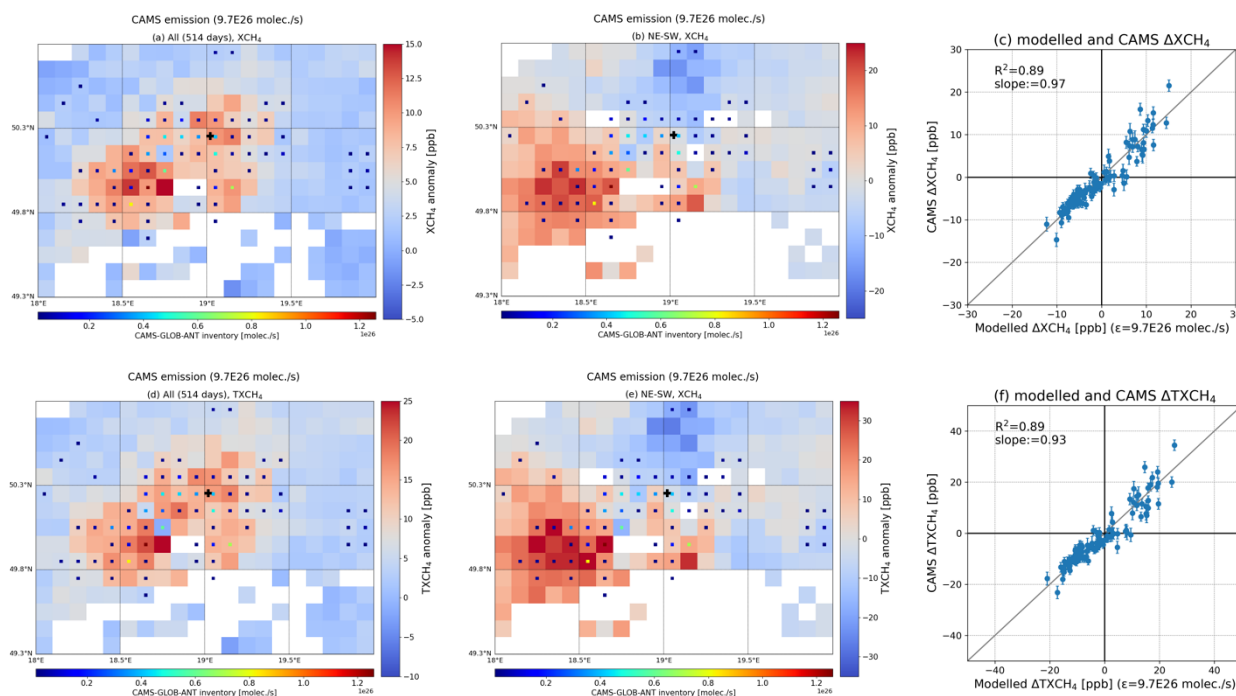
210 The retrieved  $CH_4$  from satellite observations are based on total columns and therefore, these are strongly affected by the stratospheric abundance, i.e., by the changing tropopause altitude (Liu et al, 2021; Schneider et al., 2021). The model simulation uncertainties in representing  $XCH_4$  in the stratosphere might introduce biases in investigating  $CH_4$  sources and sinks (Pandey et al., 2016). To remove this influence, we calculate the tropospheric CAMS forecasts  $CH_4$  ( $TXCH_4$ ) from the surface up to 7 km. The results are presented in Figure 5d-f. The CAMS  $TXCH_4$  anomalies have similar distribution as CAMS  $XCH_4$ , showing that background removing also works for the tropospheric  $CH_4$ . The wind-assigned plume and the correlation

215





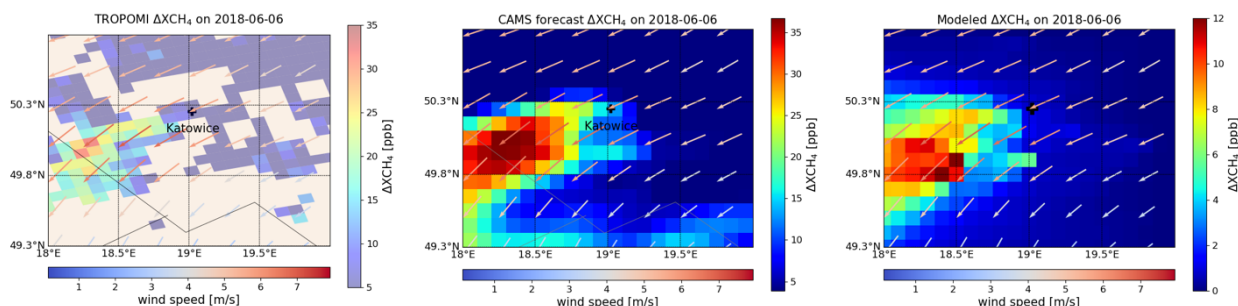
between CAMS and the wind-assigned model results are very similar between  $XCH_4$  and  $TXCH_4$ . The estimated  $CH_4$  emission strength derived from CAMS  $TXCH_4$  is  $9.1E24 \pm 1.2E24$  molec./s.



220 **Figure 5:** (a)-(c): CAMS  $XCH_4$  anomalies ( $XCH_4$ -background), the wind-assigned anomalies (NE-SW), and correlation plot between CAMS  $\Delta XCH_4$  and modelled  $\Delta XCH_4$  with using ERA5 wind at 330 m during November 2017-December 2020 over the USCB region. (d)-(f): the same as for the upper panel but for CAMS  $TXCH_4$ . The square symbols represent the locations of the CAMS-GLOB-ANT (>1E24 molec./s) inventory and different colors denote the amount of emission rates.

### 3.2 Estimated emission derived from satellite observations

225 The high-resolution TROPOMI  $XCH_4$  provides the ability to detect and quantify the  $CH_4$  emissions (e.g., oil and gas sector, coal mining) on fine and large scales (Pandey et al., 2019; Varon et al., 2019; Gouw et al., 2020; Schneising et al., 2020). Figure 6 illustrates the enhance  $XCH_4$  (raw  $XCH_4$ -background in the upwind) distribution over the USCB region on an example day (6 June 2018), in which the wind mostly came from northeast. As expected, obvious  $XCH_4$  enhancements were observed by TROPOMI along the downwind direction (southwest of Katowice where most ventilation shafts are located), as well as  
230 simulated by the CAMS forecast. The downwind-enhanced  $XCH_4$  modeled by our simple plume model and based on the CAMS-GLOB-ANT inventory also shows a similar shape of plume. This enhancement was also observed by portable FTIR instruments (COCCON) employed during the CoMet campaign (Figure 4 in Luther et al, 2019). The observations support the statement that TROPOMI is able to detect the  $CH_4$  emission signals. In addition, the downwind plume is similar to the cone-shaped plume in our simple plume model, which implies our model assumption is reasonable.



235

**Figure 6:**  $\Delta XCH_4$  together with the ERA5 wind from left: TROPOMI observations, middle: CAMS forecast at 12:00 UTC, right: from the simple plume model based on the CAMS-GLOB-ANT inventory over the USC region on an example day (6 June 2018).

Three-year averaged TROPOMI  $XCH_4$  observations presented in Figure 4b shows scattered high  $XCH_4$  amounts, whereas CAMS  $XCH_4$  is more concentrated on the center of the study area, and they agree well with its anthropogenic emission sources  
240 (CAMSGLOBANT inventory). This might be because TROPOMI detects other real  $CH_4$  sources that are not included in the CAMS forecast model data.

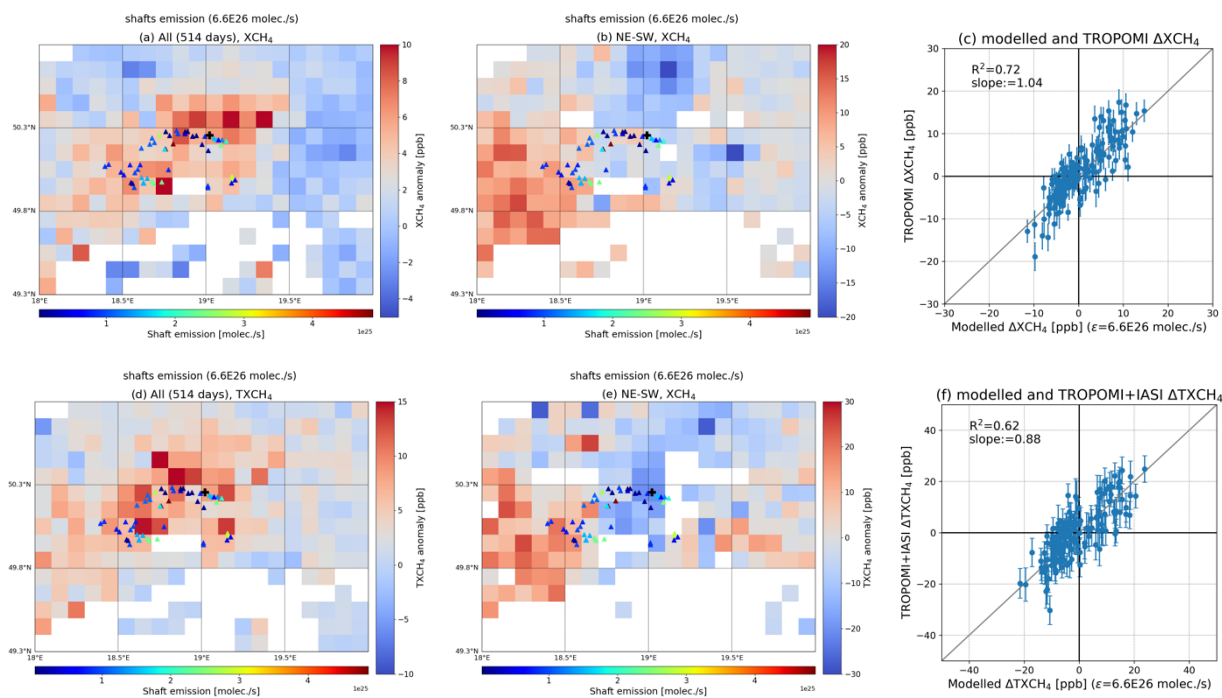
For better comparison with other studies discussing the coal mine emissions in the USC region, we apply the CoMet inventory as the a priori known sources in the wind-assigned method to estimate the  $CH_4$  emission. The results are illustrated in Figure 7. The TROPOMI  $XCH_4$  and TROPOMI+IASI  $TXCH_4$  anomalies show high amounts around the areas where the  
245 ventilation shafts are located and the region in the northeast of Katowice. Though the anomalies of the satellite observations are lower than the CAMS results (Figure 5a), their spatial distributions are similar. Positive and negative plumes can be clearly seen in Figure 7b and e. The  $\Delta XCH_4$  correlation between the TROPOMI and model have a very good agreement with a  $R^2$  value of 0.72. Similar results are also derived from TROPOMI+IASI  $TXCH_4$  with a  $R^2$  value of 0.62. Compared to CAMS  
250 sources (e.g., landfills, gas distribution network). Though none of these sources is at the same level of magnitude of coal mining emission, they might still bring some errors.

The estimated  $CH_4$  emission strengths in molec./s are  $5.7E26 \pm 4.9E24$  for  $XCH_4$  and  $5.2E26 \pm 2.2E25$  for  $TXCH_4$ , and both are close to the E-PRTR inventory ( $5.33E26$  molec./s). The TROPOMI+IASI result has a slightly higher uncertainty than the  
255 TROPOMI result, because (1) the vertical distribution of  $CH_4$  is in general much more difficult to measure than the total column of  $CH_4$  and (2) the vertical distribution is derived by considering two independent measurements, each with its own noise error. This might change for a larger number of data points (e.g., by using data from more years or by applying the method to IASI and TROPOMI successors on the upcoming METOP-SG satellite, which offers much more collocated observations).

However, in our study using  $TXCH_4$  data in addition to  $XCH_4$  data nicely documents the robustness of the method. Important  
260 for a correct estimation of the emission is the correct removal of the methane background signal. For  $XCH_4$  the stratospheric and the tropospheric backgrounds have to be removed, whereas only the tropospheric background has to be removed for

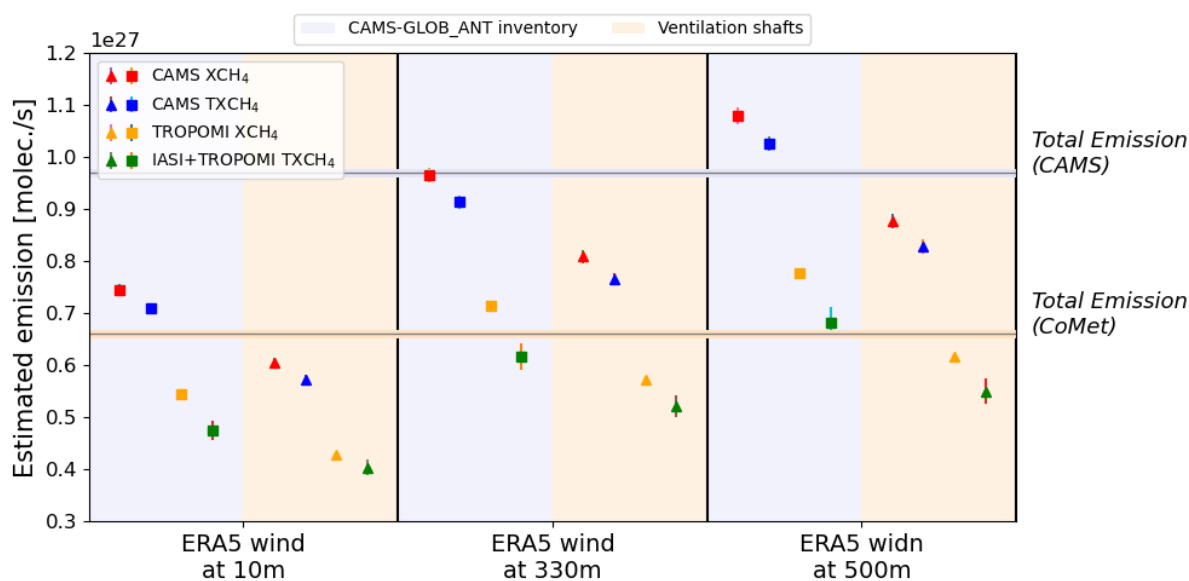


TXCH<sub>4</sub>. Despite this difference we estimate very similar emission rates from both data sets and the emission rate uncertainties of using XCH<sub>4</sub> or TXCH<sub>4</sub> are insignificant compared to the estimated emission rates.



265

**Figure 7:** Similar to Figure 5, but for (a-c) TROPOMI XCH<sub>4</sub> and (d-f) TROPOMI+IASI TXCH<sub>4</sub>. The a priori knowledge of sources are based on the CoMet inventory (Galkowski et al, 2021). The triangle symbols represent the locations of the active coal mine shafts and different colors denote the amount of emission rates.





270 **Figure 8: Estimated CH<sub>4</sub> emission rates derived from the CAMS forecasts (XCH<sub>4</sub> and TXCH<sub>4</sub>), TROPOMI XCH<sub>4</sub>, and**  
**TROPOMI+IASI TXCH<sub>4</sub> data based on different a priori knowledge of emission sources (CAMS-GLOB-ANT and CoMet**  
**inventories) and on ERA5 model winds at different altitudes (10 m, 330m, 500m). Square symbols represent the a priori emission**  
**sources from the CAMS-GLOB-ANT inventory and triangle symbols represent the a priori emission sources from the CoMet**  
**inventory. The two horizontal lines represent the number of total emissions for the CAMS-GLOB-ANT inventory (lavender color)**  
275 **and for the CoMet inventory (orange color), respectively. Note, the error bars are much smaller than the results and they are not**  
**visible here. For specific values see Table A- 2.**

### 3.3 Uncertainty analysis

Winds, particularly near the surface, are significantly altered by topography, which yields uncertainties in knowing the  
transport pathway from emission sources to the measurement location (Chen et al., 2016; Babenhauserheide et al., 2020). Thus,  
280 wind is one of the most important factors in correctly estimating the emission rates. Here we investigate the wind uncertainties  
based on the CAMS XCH<sub>4</sub> and the CAMS-GLOB-ANT inventory. The wind used in Sect. 3.3.2 and 3.3.3 are ERA5 wind at  
10 m.

#### 3.3.1 Vertical wind shear

Compared to the wind at 330 m, the wind distributions are similar at lower or higher altitude (10 m and 500 m) but the speed  
285 increases with higher altitude (Figure 3). Wind at 10 m is 19 % slower than that at 330 m (Table A- 1), which yields a  
corresponding lower estimates of  $7.4E26 \pm 1.1E25$  molec./s (-23%) based on CAMS XCH<sub>4</sub> and CAMS emission inventory  
(Figure A- 1a).

Considering the height of the Planetary Boundary Layer (PBL), we use the ERA5 wind at 500 m above the ground (Figure  
3c). The wind speed at 500 m increases by 26% and 37% for NE and SW sectors, respectively, compared to the wind at 330  
290 m. The share of SW directed winds is slightly larger at the 500 m level. These differences result in an increase of 13% of the  
estimated emission rate ( $1.1E27 \pm 1.7E25$  molec./s).

#### 3.3.2 Use of narrowed angular wind regimes

The long-term wind comes from all directions (0°-360°) (Figure 3). To define the uncertainty of wind regimes' coverage, the  
wind is separated into two groups with narrow coverage fields: NE\_narrow (0°-90°) – SW\_narrow (180°-270°) and  
295 NW\_narrow (270°-360°) – SE\_narrow (90°-180°). The final estimated emission strength is weighted by the number of the  
valid binning data in the plume maps under different wind regimes (i.e. 171 for narrow NE-SW and 26 for narrow NW-SE,  
respectively). The XCH<sub>4</sub> anomalies and the plume for narrow NE-SW regime are quite similar to those with using wider-  
coverage NE and SW fields (Figure 9a-c). CAMS  $\Delta$ XCH<sub>4</sub> and modelled  $\Delta$ XCH<sub>4</sub> show very good agreement as well. Slightly  
less data points are found here because of the choice of narrower wind fields, especially for NW-SE wind fields. The estimated  
300 emission rate is about  $9.8E26 \pm 1.5E25$  molec./s for the narrow NE-SW field. This indicates that the effect of the section in  
the wind field coverage is negligible when there are enough measurements. The use of narrow NW-SE wind fields yield an  
emission strength of  $1.4E27 \pm 5.40E25$  molec./s. The higher uncertainty is probably due to less measurements in these wind



fields. The weighted rate is therefore about  $1.0E27$  molec./s, 4.2% higher than based on the wider NE-SW wind regime (Sec. 3.1).

305

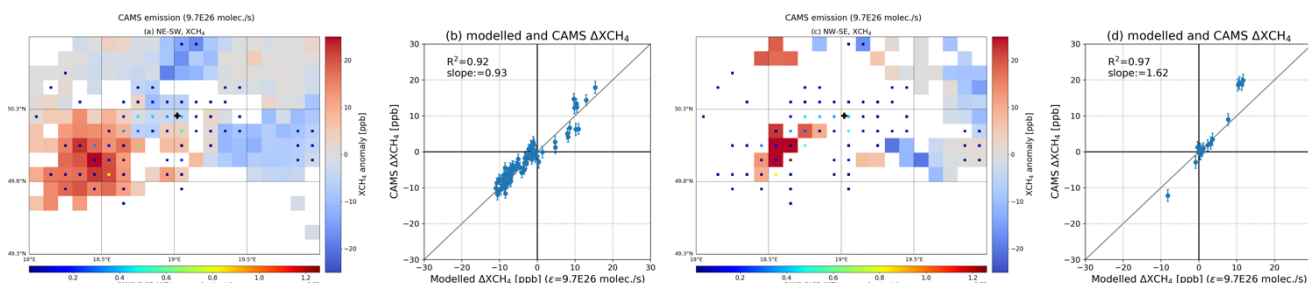


**Figure 9:** Similar figures to Figure 5b-c. Results are derived from CAMS XCH<sub>4</sub>, CAMS emission inventory and ERA5 wind at 330 m for (a)-(b) narrow wind coverage (NE\_narrow and SW\_narrow), and (c)-(d) narrow wind coverage (NW\_narrow and SE\_narrow).

### 3.3.3 Investigation of different choices for wind field segmentation

310 The wind category here is based on its predominant wind fields over the USCB region and is divided into two opposite sectors (SW and NE). To investigate its uncertainty, we apply another kind of segmentation: N (<90° or >270°) and S (90° - 270°) categories. Similar results are found and are shown in Figure 10. Though the 2D distribution of the plume changes due to the new wind category, an obvious plume can be seen. The estimated emission rate is  $9.4E26 \pm 1.7E25$  molec./s, which is only 2.1% less than that using NE and SW wind categories. The correlation between the CAMS ΔXCH<sub>4</sub> and the wind-assign-  
315 modeled ΔXCH<sub>4</sub> shows a very good agreement as well, with a similar R<sup>2</sup> value of 0.9 to that in the NE-SW wind category. This result demonstrates that our method is not significantly influenced by the wind regime division.

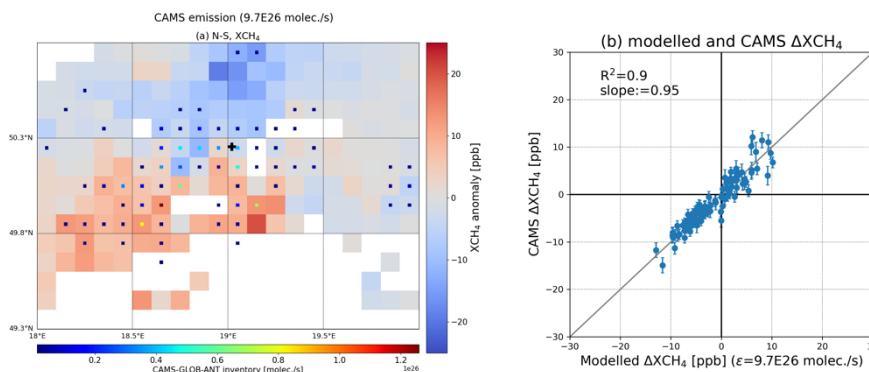


**Figure 10:** Similar figures to Figure 5b-c. Results are derived from CAMS XCH<sub>4</sub>, CAMS emission inventory and ERA5 wind at 330 m but using a new wind category (N and S).

## 320 4. Conclusion

Intensive mining activities are the dominant CH<sub>4</sub> emission sources in the USCB region, Poland, where one of the largest coal mining areas in Europe is located. It is thus of importance to quantify the CH<sub>4</sub> emissions from this area. In this study we use



the combination of a simple plume model and a novel wind-assigned model to estimate CH<sub>4</sub> emission rates from high-resolution CAMS forecast XCH<sub>4</sub> and TXCH<sub>4</sub>, along with satellite data (TROPOMI XCH<sub>4</sub> and TROPOMI+IASI TXCH<sub>4</sub>) over  
325 the USCB region (49.3°N-50.8°N and 18°E-20°E) from November 2017 to December 2020.

Based on the CAMS-GLOB-ANT inventory, the dominant CH<sub>4</sub> source is emitted from energy production and distribution, and the significant sources are spread around the city of Katowice and its southwest region. We firstly apply the wind-assigned method to the CAMS forecasts based on the a priori knowledge of CAMS-GLOB-ANT inventory (9.7E26 molec./s in total) and ERA5 wind at ~330 m. We use  $\Delta XCH_4/\Delta TXCH_4$  to represent the difference of XCH<sub>4</sub>/TXCH<sub>4</sub> between the conditions of  
330 two opposite wind fields (NE and SW). The CAMS  $\Delta XCH_4/\Delta TXCH_4$  data show very good agreements with the output of the wind-assigned anomalies with a R<sup>2</sup> value of 0.89 for CAMS XCH<sub>4</sub> and CAMS TXCH<sub>4</sub>. This nice correlation indicates that our background removal works well. In addition, similar estimates are derived from CAMS XCH<sub>4</sub> (9.6E26 ± 1.4E25 molec./s) and TXCH<sub>4</sub> (9.1E26 ± 1.2E24 molec./s).

To investigate the CH<sub>4</sub> emissions from this hot spot, the CoMet campaign was performed in 2018. Locations and emission  
335 rates of the ventilation shafts of the coal mine used in this study are based on this inventory. Based on this knowledge, the estimated CH<sub>4</sub> emissions are 5.7E26 ± 4.9E24 molec./s and 5.2E26 ± 2.2E25 molec./s derived from the TROPOMI XCH<sub>4</sub> and combined TROPOMI+IASI TXCH<sub>4</sub>, respectively. These results are 40% less than that derived from the CAMS model and CAMS-GLOB-ANT inventory. It is probably because the CAMS inventory includes many sectors of anthropogenic sources, like wastes, and combustion from residential and commercial, which account for about 20%. Nevertheless, our results derived  
340 from satellite observations are close to the E-PRTR inventory of 5.33E26 molec./s and reasonably compared to the CoMet inventory (6.6E26 molec./s), and to previous studies over the USCB region (ranging from 1.05E25 molec./s to 9.38E25 molec./s for a sub-clusters of shafts (Krautwurst et al., 2021) up to 5.68E26 molec./s derived from one flight (Kostinek et al. (2021)). Similar 2D anomalies and plumes are also observed for TROPOMI XCH<sub>4</sub> and TROPOMI+IASI TXCH<sub>4</sub>. This nicely documents the robustness of the method. The TROPOMI+IASI result has a slightly higher uncertainty than the TROPOMI  
345 result, because (1) the vertical distribution of CH<sub>4</sub> is in general much more difficult to measure than the total column of CH<sub>4</sub> and (2) the vertical distribution is derived by considering two independent measurements, each with its own noise error. This might change for a larger number of data points (e.g. by using data from more years or by applying the method to IASI and TROPOMI successors on the upcoming METOP-SG satellite, which offers much more collocated observations). Nonetheless, the uncertainties are insignificant compared to the estimated emission rates.

350 Wind contains uncertainties in knowing the transport pathway from emission sources to the measurement location and thus, we analyze the effects in selecting wind at lower and higher altitude (10 m and 500 m), wind field coverage and wind category. Wind distributions at higher levels are similar to that at 330 m. However, their speeds decrease by 19% at 10 m and increase by 32% at 500 m, which results in higher emission rates by -23% and 13 %, respectively. Narrower wind field coverage (0°-90° for NE sector and 180°-270° for SW sector) and different wind segmentation (<90° or >270° for N sector and 90°-270°  
355 for S sector) introduce minor uncertainties of +4.2 % and -2.1 %, respectively. The agreements for these sensitivity tests between the CAMS  $\Delta XCH_4$  and wind-assigned model  $\Delta XCH_4$  are as good as that using previous NE and SW wind fields. The



results suggest that our method is robust since it is insensitive to the separation of the wind regimes. It is also suitable for estimating CH<sub>4</sub> and CO<sub>2</sub> emissions in other regions.

360 *Data availability.* The data are accessible by contacting the corresponding author (qiansi.tu@kit.edu). The SRON S5P-RemoTeC scientific TROPOMI CH<sub>4</sub> dataset from this study is available for download at <https://doi.org/10.5281/zenodo.4447228> (Lorente et al., 2021, last access: 08 November 2021). The TROPOMI data set is publicly available from <https://scihub.copernicus.eu/> (last access: 08 November 2021; ESA, 2020). The access and use of any Copernicus Sentinel data available through the Copernicus Open Access Hub are governed by the legal notice on the use of  
365 Copernicus Sentinel Data and Service Information, which is given here: [https://sentinels.copernicus.eu/documents/247904/690755/Sentinel\\_Data\\_Legal\\_Notice](https://sentinels.copernicus.eu/documents/247904/690755/Sentinel_Data_Legal_Notice) (last access: 08 November 2021; European Commission, 2020). The MUSICA IASI data set is available for download via <https://doi.org/10.35097/408> (Schneider et al. 2021).

370 *Author contributions.* Qiansi Tu, Frank Hase and Matthias Schneider developed the research question. Qiansi Tu wrote the manuscript and performed the data analysis with input from Frank Hase, Matthias Schneider and Farahnaz Khosrawi. Matthias Schneider, Benjamin Ertl and Christopher J. Diekmann provided the combined (MUSICA IASI + TROPOMI) data and supported technically for the analysis of these data. Jarosław Necki supported in consultation of the local situation and CoMet inventory. All authors discussed the results and contributed to the final manuscript.

375 *Competing interests.* The authors declare that they have no conflict of interest.

*Acknowledgements.* The CAMS results were generated using Copernicus Atmosphere Monitoring Service (2017–2020) information. Neither the European Commission nor ECMWF is responsible for any use that may be made of the Copernicus  
380 information or data it contains. We also thank Michela Giusti and Kevin Marsh in the Data Support Team at ECMWF for retrieving and providing comments about the CAMS data. This research has largely benefit from funds of the Deutsche Forschungsgemeinschaft (provided for the two projects MOTIV and TEDDY with IDs/290612604 and 416767181, respectively). Important part of this work was performed on the supercomputer ForHLR funded by the Ministry of Science, Research and the Arts Baden-Württemberg and by the German Federal Ministry of Education and Research. We acknowledge  
385 Emissions of atmospheric Compounds and Compilation of Ancillary Data (ECCAD) for providing CAMS-GLOB-ANT inventory data.

We acknowledge the support by the Deutsche Forschungsgemeinschaft and the Open Access Publishing Fund of the Karlsruhe Institute of Technology.

390



## Appendix

**Table A- 1: Number of days and the averaged wind speed ( $\pm$  standard deviation) per specific wind area in daytime (08:00 UTC – 18:00 UTC) at different vertical levels from November 2017 to December 2020 over the USCB region. Days are coincided with days with TROPOMI overpass days.**

	NE / $>315^\circ$ or $<135^\circ$		SW / $135^\circ - 315^\circ$	
	Number of days in total (%)	Averaged wind speed $\pm$ standard deviation ( $\text{m s}^{-1}$ )	Number of days in total (%)	Averaged wind speed $\pm$ standard deviation ( $\text{m s}^{-1}$ )
10 m	40.4	$3.4 \pm 1.6$	52.0	$3.5 \pm 1.7$
$\sim 330$ m (975 hPa)	40.4	$4.2 \pm 2.3$	51.4	$4.3 \pm 2.4$
$\sim 500$ m (950 hPa)	40.2	$5.3 \pm 2.9$	53.0	$5.9 \pm 3.5$

395

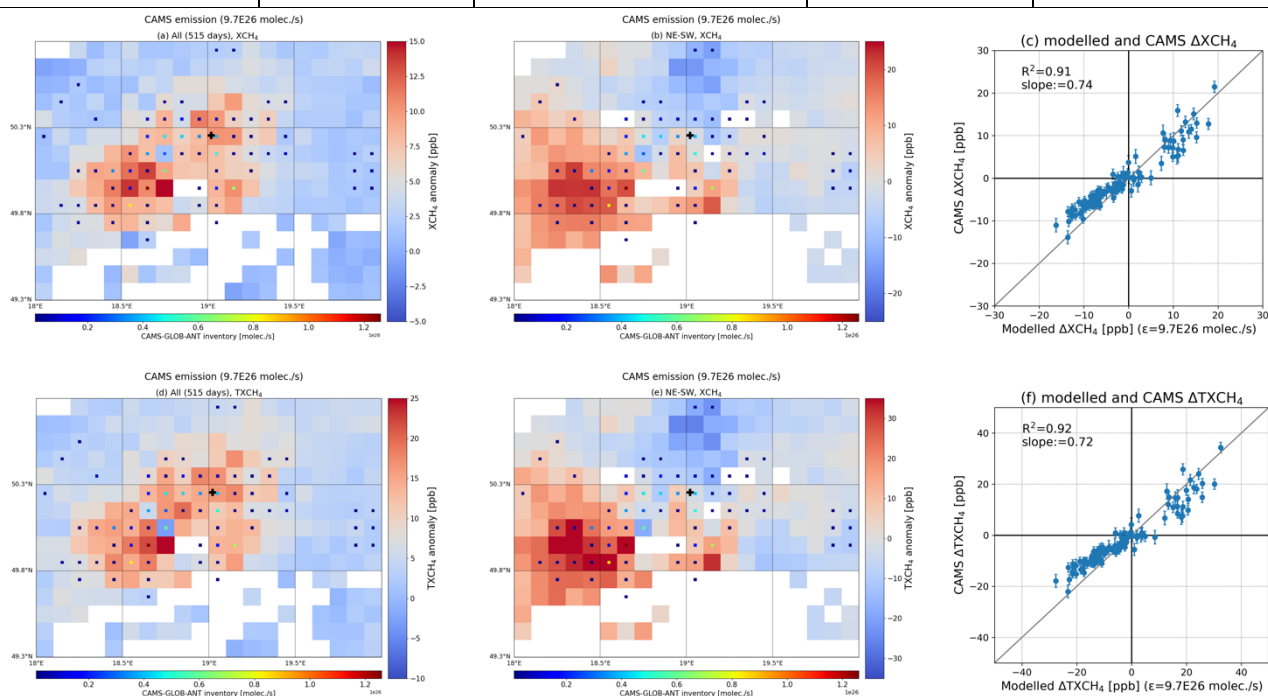


**Figure A- 1: Similar to Figure 5 but using ERA5 wind at 10 m.**

400





405 **Table A- 2: Estimated CH<sub>4</sub> emission rates derived from CAMS forecasts (XCH<sub>4</sub> and TXCH<sub>4</sub>), TROPOMI XCH<sub>4</sub>, and IASI&TROPOMI TXCH<sub>4</sub> data based on different a priori knowledge of emission sources (CAMS-GLOB-ANT and CoMet campaign inventories) and ERA5 model winds at different altitudes (10 m, 100 m and ~500 m).**

	ERA5 wind at 10 m		ERA5 wind at 330 m (975 hPa)		ERA5 wind at 500 m (950 hPa)	
	CAMS emission (total = 9.7E26 molec./s)	shafts emission (total = 6.6E26 molec./s)	CAMS emission (total = 9.7E26 molec./s)	shafts emission (total = 6.6E26 molec./s)	CAMS emission (total = 9.7E26 molec./s)	shafts emission (total = 6.6E26 molec./s)
CAMS XCH <sub>4</sub>	7.4E26 ± 1.1E25	6.1E26 ± 9.5E24	9.6E26 ± 1.4E25	8.1E26 ± 1.3E25	1.1E27 ± 1.7E25	8.8E26 ± 1.4E25
CAMS TXCH <sub>4</sub>	7.1E26 ± 9.4E24	5.7E26 ± 8.3E24	9.1E26 ± 1.2E25	7.7E26 ± 1.1E25	1.0E27 ± 1.5E25	8.3E26 ± 1.3E25
TROPOMI XCH <sub>4</sub>	5.4E26 ± 4.4E24	4.3E26 ± 3.6E24	7.1E26 ± 5.8E24	5.7E26 ± 4.9E24	7.8E26 ± 6.5E24	6.2E26 ± 5.5E24
IASI&TROPOMI TXCH <sub>4</sub>	4.7E26 ± 1.9E25	4.0E26 ± 1.6E25	6.2E26 ± 2.5E25	5.2E26 ± 2.2E25	6.8E26 ± 2.9E25	5.5E26 ± 2.4E25



## 410 References

- Agustí-Panareda, A., Diamantakis, M., Massart, S., Chevallier, F., Muñoz-Sabater, J., Barré, J., Curcoll, R., Engelen, R., Langerock, B., Law, R. M., Loh, Z., Morguí, J. A., Parrington, M., Peuch, V.-H., Ramonet, M., Roehl, C., Vermeulen, A. T., Warneke, T., and Wunch, D.: Modelling CO<sub>2</sub> weather – why horizontal resolution matters, *Atmos. Chem. Phys.*, 19, 7347–7376, <https://doi.org/10.5194/acp-19-7347-2019>, 2019.
- 415 Andersen, T., Vinkovic, K., de Vries, M., Kers, B., Necki, J., Swolkien, J., Roiger, A., Peters, W. and Chen, H.: Quantifying methane emissions from coal mining ventilation shafts using an unmanned aerial vehicle (UAV)-based active AirCore system, *Atmos. Environ. X*, 12, 100135, doi:<https://doi.org/10.1016/j.aeaoa.2021.100135>, 2021.
- Babenhauserheide, A., Hase, F., and Morino, I.: Net CO<sub>2</sub> fossil fuel emissions of Tokyo estimated directly from measurements of the Tsukuba TCCON site and radiosondes, *Atmos. Meas. Tech.*, 13, 2697–2710, [https://doi.org/10.5194/amt-13-](https://doi.org/10.5194/amt-13-2697-2020)  
420 2697-2020, 2020.
- Barré, J., Aben, I., Agustí-Panareda, A., Balsamo, G., Bousserez, N., Dueben, P., Engelen, R., Inness, A., Lorente, A., McNorton, J., Peuch, V.-H., Radnoti, G., and Ribas, R.: Systematic detection of local CH<sub>4</sub> anomalies by combining satellite measurements with high-resolution forecasts, *Atmos. Chem. Phys.*, 21, 5117–5136, <https://doi.org/10.5194/acp-21-5117-2021>, 2021.
- 425 Boesch, H., Baker, D., Connor, B., Crisp, D. and Miller, C.: Global Characterization of CO<sub>2</sub> Column Retrievals from Shortwave-Infrared Satellite Observations of the Orbiting Carbon Observatory-2 Mission, *Remote Sens.*, 3(2), doi:10.3390/rs3020270, 2011.
- Butz, A., Hasekamp, O. P., Frankenberg, C., and Aben, I.: Retrievals of atmospheric CO<sub>2</sub> from simulated space-borne measurements of backscattered near-infrared sunlight: accounting for aerosol effects, *Appl. Opt.* 48, 3322–3336,  
430 2009.
- Butz, A., Hasekamp, O. P., Frankenberg, C., Vidot, J. and Aben, I.: CH<sub>4</sub> retrievals from space-based solar backscatter measurements: Performance evaluation against simulated aerosol and cirrus loaded scenes, *J. Geophys. Res. Atmos.*, 115(D24), doi:<https://doi.org/10.1029/2010JD014514>, 2010.
- Butz, A., Guerlet, S., Hasekamp, O., Schepers, D., Galli, A., Aben, I., Frankenberg, C., Hartmann, J.-M., Tran, H., Kuze, A.,  
435 Keppel-Aleks, G., Toon, G., Wunch, D., Wennberg, P., Deutscher, N., Griffith, D., Macatangay, R., Messerschmidt, J., Notholt, J., and Warneke, T.: Toward accurate CO<sub>2</sub> and CH<sub>4</sub> observations from GOSAT, *Geophysical Research Letters*, 38, <https://doi.org/10.1029/2011GL047888>, <https://agupubs.onlinelibrary.wiley.com/doi/abs/10.1029/2011GL047888>, 2011.
- Chen, J., Viatte, C., Hedelius, J. K., Jones, T., Franklin, J. E., Parker, H., Gottlieb, E. W., Wennberg, P. O., Dubey, M. K., and  
440 595 Wofsy, S. C.: Differential column measurements using compact solar-tracking spectrometers, *Atmos. Chem. Phys.*, 16, 8479–8498, <https://doi.org/10.5194/acp-16-8479-2016>, 2016.



- Copernicus Climate Change Service (C3S): ERA5: Fifth generation of ECMWF atmospheric reanalyses of the global climate. Copernicus Climate Change Service Climate Data Store (CDS), date of access. <https://cds.climate.copernicus.eu/cdsapp#!/home>, 2017.
- 445 Crippa, M., Guizzardi, D., Muntean, M., Schaaf, E., Dentener, F., van Aardenne, J. A., Monni, S., Doering, U., Olivier, J. G. J., Pagliari, V., and Janssens-Maenhout, G.: Gridded emissions of air pollutants for the period 1970–2012 within EDGAR v4.3.2, *Earth Syst. Sci. Data*, 10, 1987–2013, <https://doi.org/10.5194/essd-10-1987-2018>, 2018.
- Fiehn, A., Kostinek, J., Eckl, M., Klausner, T., Gałkowski, M., Chen, J., Gerbig, C., Röckmann, T., Maazallahi, H., Schmidt, M., Korbeń, P., Nečki, J., Jagoda, P., Wildmann, N., Mallaun, C., Bun, R., Nickl, A.-L., Jöckel, P., Fix, A., and  
450 Roiger, A.: Estimating CH<sub>4</sub>, CO<sub>2</sub> and CO emissions from coal mining and industrial activities in the Upper Silesian Coal Basin using an aircraft-based mass balance approach, *Atmos. Chem. Phys.*, 20, 12675–12695, <https://doi.org/10.5194/acp-20-12675-2020>, 2020.
- Flemming, J., Huijnen, V., Arteta, J., Bechtold, P., Beljaars, A., Blechschmidt, A.-M., Diamantakis, M., Engelen, R. J., Gaudel, A., Inness, A., Jones, L., Josse, B., Katragkou, E., Marecal, V., Peuch, V.-H., Richter, A., Schultz, M. G., Stein, O.,  
455 and Tsikerdekis, A.: Tropospheric chemistry in the Integrated Forecasting System of ECMWF, *Geosci. Model Dev.*, 8, 975–1003, <https://doi.org/10.5194/gmd-8-975-2015>, 2015.
- De Gouw, J. A., Veeffkind, J. P., Roosenbrand, E., Dix, B., Lin, J. C., Landgraf, J., and Levelt, P. F.: Daily Satellite Observations of Methane from Oil and Gas Production Regions in the United States, *Scientific Reports*, 10, 1379, <https://doi.org/10.1038/s41598-020-57678-4>, 2020.
- 460 Gałkowski, M., Fiehn, A., Swolkien, J., Stanisavljevic, M., Korben, P., Menoud, M., Necki, J., Roiger, A., Röckmann, T., Gerbig, C., & Fix, A. (2021). Emissions of CH<sub>4</sub> and CO<sub>2</sub> over the Upper Silesian Coal Basin (Poland) and its vicinity (4.01) [Data set]. ICOS ERIC - Carbon Portal. <https://doi.org/10.18160/3K6Z-4H73>.
- Granier, C., S. Darras, H. Denier van der Gon, J. Doubalova, N. Elguindi, B. Galle, M. Gauss, M. Guevara, J.-P. Jalkanen, J. Kuenen, C. Liousse, B. Quack, D. Simpson, K. Sindelarova, The Copernicus Atmosphere Monitoring Service global  
465 and regional emissions (April 2019 version), Copernicus Atmosphere Monitoring Service (CAMS) report, doi:10.24380/d0bn-kx16, 2019.
- Hasekamp, O. P., and Butz, A.: Efficient calculation of intensity and polarization spectra in vertically inhomogeneous scattering and absorbing atmospheres, *J. Geophys. Res.*, 113, D20309, doi:10.1029/2008JD010379, 2008.
- Hasekamp, O., Lorente, A., Hu, H., Butz, A., aan de Brugh, J., and Landgraf, J.: Algorithm Theoretical Baseline Document  
470 for Sentinel-5 Precursor methane retrieval, <http://www.tropomi.eu/documents/atbd/>, 2019.
- Hersbach, H., Bell, B., Berrisford, P., Hirahara, S., Horányi, A., Muñoz-Sabater, J., Nicolas, J., Peubey, C., Radu, R., Schepers, D., Simmons, A., Soci, C., Abdalla, S., Abellan, X., Balsamo, G., Bechtold, P., Biavati, G., Bidlot, J., Bonavita, M., De Chiara, G., Dahlgren, P., Dee, D., Diamantakis, M., Dragani, R., Flemming, J., Forbes, R., Fuentes, M., Geer, A., Haimberger, L., Healy, S., Hogan, R. J., Hólm, E., Janisková, M., Keeley, S., Laloyaux, P., Lopez, P., Lupu, C.,



- 475 Radnoti, G., de Rosnay, P., Rozum, I., Vamborg, F., Villaume, S. and Thépaut, J.-N.: The ERA5 global reanalysis, *Q. J. R. Meteorol. Soc.*, 146(730), 1999–2049, doi:<https://doi.org/10.1002/qj.3803>, 2020.
- Hoesly, R. M., Smith, S. J., Feng, L., Klimont, Z., Janssens-Maenhout, G., Pitkanen, T., Seibert, J. J., Vu, L., Andres, R. J., Bolt, R. M., Bond, T. C., Dawidowski, L., Kholod, N., Kurokawa, J.-I., Li, M., Liu, L., Lu, Z., Moura, M. C. P., O'Rourke, P. R., and Zhang, Q.: Historical (1750–2014) anthropogenic emissions of reactive gases and aerosols from the Community Emissions Data System (CEDS), *Geosci. Model Dev.*, 11, 369–408, <https://doi.org/10.5194/gmd-11-369-2018>, 2018.
- 480 Kirschke, S., Bousquet, P., Ciais, P., Saunoy, M., Canadell, J. G., Dlugokencky, E. J., Bergamaschi, P., Bergmann, D., Blake, D. R., Bruhwiler, L., Cameron-Smith, P., Castaldi, S., Chevallier, F., Feng, L., Fraser, A., Heimann, M., Hodson, E. L., Houweling, S., Josse, B., Fraser, P. J., Krummel, P. B., Lamarque, J.-F., Langenfelds, R. L., Le Quéré, C., Naik, V., O'Doherty, S., Palmer, P. I., Pison, I., Plummer, D., Poulter, B., Prinn, R. G., Rigby, M., Ringeval, B., Santini, M., Schmidt, M., Shindell, D. T., Simpson, I. J., Spahni, R., Steele, L. P., Strode, S. A., Sudo, K., Szopa, S., van der Werf, G. R., Voulgarakis, A., van Weele, M., Weiss, R. F., Williams, J. E. and Zeng, G.: Three decades of global methane sources and sinks, *Nat. Geosci.*, 6(10), 813–823, doi:10.1038/ngeo1955, 2013.
- 485 Kostinek, J., Roiger, A., Eckl, M., Fiehn, A., Luther, A., Wildmann, N., Klausner, T., Fix, A., Knote, C., Stohl, A., and Butz, A.: Estimating Upper Silesian coal mine methane emissions from airborne in situ observations and dispersion modeling, *Atmos. Chem. Phys.*, 21, 8791–8807, <https://doi.org/10.5194/acp-21-8791-2021>, 2021.
- Krautwurst, S., Gerilowski, K., Borchardt, J., Wildmann, N., Galkowski, M., Swolkien, J., Marshall, J., Fiehn, A., Roiger, A., Ruutz, T., Gerbig, C., Necki, J., Burrows, J. P., Fix, A., and Bovensmann, H.: Quantification of CH<sub>4</sub> coal mining emissions in Upper Silesia by passive airborne remote sensing observations with the MAMAP instrument during CoMet, *Atmos. Chem. Phys. Discuss.* [preprint], <https://doi.org/10.5194/acp-2020-1014>, in review, 2021.
- 495 Landgraf, J., Butz, A., Hasekamp, O., Hu, H., and aan de Brugh, J.: Sentinel 5 L2 Prototype Processors, Algorithm Theoretical Baseline Document: Methane Retrieval, 2019.
- Liu, M., van der A, R., van Weele, M., Eskes, H., Lu, X., Veeffkind, P., de Laat, J., Kong, H., Wang, J., Sun, J., Ding, J., Zhao, Y. and Weng, H.: A New Divergence Method to Quantify Methane Emissions Using Observations of Sentinel-5P TROPOMI, *Geophys. Res. Lett.*, 48(18), e2021GL094151, doi:<https://doi.org/10.1029/2021GL094151>, 2021.
- 500 Lorente, A., Borsdorff, T., Butz, A., Hasekamp, O., aan de Brugh, J., Schneider, A., Wu, L., Hase, F., Kivi, R., Wunch, D., Pollard, D. F., Shiomi, K., Deutscher, N. M., Velasco, V. A., Roehl, C. M., Wennberg, P. O., Warneke, T., and Landgraf, J.: Methane retrieved from TROPOMI: improvement of the data product and validation of the first 2 years of measurements, *Atmos. Meas. Tech.*, 14, 665–684, <https://doi.org/10.5194/amt-14-665-2021>, 2021.
- 505 Luther, A., Kleinschek, R., Scheidweiler, L., Defratyka, S., Stanisavljevic, M., Forstmaier, A., Dandocsi, A., Wolff, S., Dubravica, D., Wildmann, N., Kostinek, J., Jöckel, P., Nickl, A.-L., Klausner, T., Hase, F., Frey, M., Chen, J., Dietrich, F., Nećki, J., Swolkien, J., Fix, A., Roiger, A., and Butz, A.: Quantifying C<sub>4</sub> emissions from hard coal



- mines using mobile sun-viewing Fourier transform spectrometry, *Atmos. Meas. Tech.*, 12, 5217–5230, <https://doi.org/10.5194/amt-12-5217-2019>, 2019.
- 510 Luther, A., Kostinek, J., Kleinschek, R., Defratyka, S., Stanisavljevic, M., Forstmaier, A., Dandocsi, A., Scheidweiler, L., Dubravica, D., Wildmann, N., Hase, F., Frey, M. M., Chen, J., Dietrich, F., Necki, J., Swolkien, J., Knote, C., Vardag, S. N., Roiger, A., and Butz, A.: Observational constraints on methane emissions from Polish coal mines using a ground-based remote sensing network, *Atmos. Chem. Phys. Discuss.* [preprint], <https://doi.org/10.5194/acp-2021-978>, in review, 2021.
- 515 Pandey, S., Houweling, S., Krol, M., Aben, I., Chevallier, F., Dlugokencky, E. J., Gatti, L. V., Gloor, E., Miller, J. B., Detmers, R., Machida, T., and Röckmann, T.: Inverse modeling of GOSAT-retrieved ratios of total column CH<sub>4</sub> and CO<sub>2</sub> for 2009 and 2010, *Atmos. Chem. Phys.*, 16, 5043–5062, <https://doi.org/10.5194/acp-16-5043-2016>, 2016.
- Pandey, S., Gautam, R., Houweling, S., van der Gon, H. D., Sadavarte, P., Borsdorff, T., Hasekamp, O., Landgraf, J., Tol, P., van Kempen, T., Hoogeveen, R., van Hees, R., Hamburg, S. P., Maasakkers, J. D., and Aben, I.: Satellite observations  
520 reveal extreme methane leakage from a natural gas well blowout, *Proc Natl Acad Sci USA*, 116, 26376, <https://doi.org/10.1073/pnas.1908712116>, 2019.
- Prather, M. J., Holmes, C. D. and Hsu, J.: Reactive greenhouse gas scenarios: Systematic exploration of uncertainties and the role of atmospheric chemistry, *Geophys. Res. Lett.*, 39(9), doi:<https://doi.org/10.1029/2012GL051440>, 2012.
- IPCC, 2014: Climate Change 2014: Synthesis Report. Contribution of Working Groups I, II and III to the Fifth Assessment  
525 Report of the Intergovernmental Panel on Climate Change [Core Writing Team, R.K. Pachauri and L.A. Meyer (eds.)]. IPCC, Geneva, Switzerland, 151 pp.
- Saunois, M., Stavert, A. R., Poulter, B., Bousquet, P., Canadell, J. G., Jackson, R. B., Raymond, P. A., Dlugokencky, E. J., Houweling, S., Patra, P. K., Ciais, P., Arora, V. K., Bastviken, D., Bergamaschi, P., Blake, D. R., Brailsford, G., Bruhwiler, L., Carlson, K. M., Carrol, M., Castaldi, S., Chandra, N., Crevoisier, C., Crill, P. M., Covey, K., Curry, C.  
530 L., Etiope, G., Frankenberg, C., Gedney, N., Hegglin, M. I., Höglund-Isaksson, L., Hugelius, G., Ishizawa, M., Ito, A., Janssens-Maenhout, G., Jensen, K. M., Joos, F., Kleinen, T., Krummel, P. B., Langenfelds, R. L., Laruelle, G. G., Liu, L., Machida, T., Maksyutov, S., McDonald, K. C., McNorton, J., Miller, P. A., Melton, J. R., Morino, I., Müller, J., Murguía-Flores, F., Naik, V., Niwa, Y., Noce, S., O'Doherty, S., Parker, R. J., Peng, C., Peng, S., Peters, G. P., Prigent, C., Prinn, R., Ramonet, M., Regnier, P., Riley, W. J., Rosentreter, J. A., Segers, A., Simpson, I. J., Shi, H.,  
535 Smith, S. J., Steele, L. P., Thornton, B. F., Tian, H., Tohjima, Y., Tubiello, F. N., Tsuruta, A., Viovy, N., Voulgarakis, A., Weber, T. S., van Weele, M., van der Werf, G. R., Weiss, R. F., Worthy, D., Wunch, D., Yin, Y., Yoshida, Y., Zhang, W., Zhang, Z., Zhao, Y., Zheng, B., Zhu, Q., Zhu, Q., and Zhuang, Q.: The Global Methane Budget 2000–2017, *Earth Syst. Sci. Data*, 12, 1561–1623, <https://doi.org/10.5194/essd-12-1561-2020>, 2020.
- Schneider, M., Ertl, B., Diekmann, C. J., Khosrawi, F., Röhling, A. N., Hase, F., Dubravica, D., García, O. E., Sepúlveda, E.,  
540 Borsdorff, T., Landgraf, J., Lorente, A., Chen, H., Kivi, R., Laemmle, T., Ramonet, M., Crevoisier, C., Pernin, J., Steinbacher, M., Meinhardt, F., Deutscher, N. M., Griffith, D. W. T., Velazco, V. A., and Pollard, D. F.: Synergetic



- use of IASI and TROPOMI space borne sensors for generating a tropospheric methane profile product, *Atmos. Meas. Tech. Discuss.* [preprint], <https://doi.org/10.5194/amt-2021-31>, in review, 2021.
- 545 Schepers, D., Guerlet, S., Butz, A., Landgraf, J., Frankenberg, C., Hasekamp, O., Blavier, J.-F., Deutscher, N. M., Griffith, D. W. T., Hase, F., Kyro, E., Morino, I., Sherlock, V., Sussmann, R. and Aben, I.: Methane retrievals from Greenhouse Gases Observing Satellite (GOSAT) shortwave infrared measurements: Performance comparison of proxy and physics retrieval algorithms, *J. Geophys. Res. Atmos.*, 117(D10), doi:<https://doi.org/10.1029/2012JD017549>, 2012.
- 550 Schneising, O., Buchwitz, M., Reuter, M., Vanselow, S., Bovensmann, H., and Burrows, J. P.: Remote sensing of methane leakage from natural gas and petroleum systems revisited, *Atmos. Chem. Phys.*, 20, 9169–9182, <https://doi.org/10.5194/acp-20-9169-2020>, 2020.
- Tu, Q., Hase, F., Schneider, M., García, O., Blumenstock, T., Borsdorff, T., Frey, M., Khosrawi, F., Lorente, A., Alberti, C., Bustos, J. J., Butz, A., Carreño, V., Cuevas, E., Curcoll, R., Diekmann, C. J., Dubravica, D., Ertl, B., Estruch, C., León-Luis, S. F., Marrero, C., Morgui, J.-A., Ramos, R., Scharun, C., Schneider, C., Sepúlveda, E., Toledano, C., and Torres, C.: Quantification of CH<sub>4</sub> emissions from waste disposal sites near the city of Madrid using ground- and space-based observations of COCCON, TROPOMI and IASI, *Atmos. Chem. Phys. Discuss.* [preprint], <https://doi.org/10.5194/acp-2021-437>, in review, 2021.
- 555 Varon, D. J., McKeever, J., Jervis, D., Maasackers, J. D., Pandey, S., Houweling, S., Aben, I., Scarpelli, T. and Jacob, D. J. : Satellite discovery of anomalously large methane point sources from oil/gas production, *Geophysical Research Letters*, 46, 13507– 13516. <https://doi.org/10.1029/2019GL083798>, 2019.
- 560 Veefkind, J. P., Aben, I., McMullan, K., Förster, H., de Vries, J., Otter, G., Claas, J., Eskes, H. J., de Haan, J. F., Kleipool, Q., van Weele, M., Hasekamp, O., Hoogeveen, R., Landgraf, J., Snel, R., Tol, P., Ingmann, P., Voors, R., Kruizinga, B., Vink, R., Visser, H., and Levelt, P. F.: TROPOMI on the ESA Sentinel-5 Precursor: A GMES mission for global observations of the atmospheric composition for climate, air quality and ozone layer applications, *Remote Sens. Environ.*, 120, 70–83, <https://doi.org/10.1016/j.rse.2011.09.027>, 2012.

565